PHYSICAL REVIEW B **67**, 035405 (2003)

Comparative study of Si(001) surface structure and interatomic potentials in finite-temperature simulations

L. Nurminen,[1] F. Tavazza,[2] D. P. Landau,[1,2] A. Kuronen,[1] and K. Kaski[1]
[1]*Laboratory of Computational Engineering, Helsinki University of Technology, P.O. Box 9203, 02015 Helsinki, Finland*
[2]*Center for Simulational Physics, The University of Georgia, Athens, Georgia 30602-2451*

(Received 16 August 2002; revised manuscript received 2 October 2002; published 14 January 2003)

We have performed a comparative study of three widely used classical many-body potentials for silicon (Stillinger-Weber, Tersoff-2, and Tersoff-3) in connection with finite-temperature simulations of the Si(001) surface. Large-scale constant-pressure Monte Carlo simulations are used to examine the reconstruction of the Si(001) surface, formation of antiphase boundaries, and defect structures such as dimer vacancies. The accuracy of the empirical potentials is compared with first-principles methods and with experimental results when possible. We find that good performance in the static limit (i.e., at $T=0$ K) does not ensure the suitability of the potential for finite-temperature simulations. The Stillinger-Weber potential is found to give the best overall performance.

DOI: 10.1103/PhysRevB.67.035405 PACS number(s): 68.35.Bs, 05.10.Ln

I. INTRODUCTION

Extensive efforts have been devoted to the study of the silicon (001) surface partly due to the fact that the microelectronic industry relies heavily on silicon technology and partly because silicon surface properties still pose challenges to our theoretical understanding.[1] The surface displays a variety of fascinating phenomena despite its relatively simple composition. For these reasons, Si(001) is an ideal system for developing simulation methods based on empirical many-body potentials. Accurate first-principles quantum-mechanical methods[2] are currently limited to static calculations of small systems composed of only few hundred atoms at best. Large-scale simulations are, however, required in cases where long-range elastic interactions are involved due to surface reconstructions and defects. Therefore, empirical potentials are valuable for studying both static and dynamic properties in simulations involving tens of thousands of atoms. Furthermore, the empirical approach can be used to study systems at nonzero values of temperature where entropic effects may compete with the internal energy in determining what the state of lowest free energy is.

Other techniques, such as tight binding,[3] have been developed to fill in the gap between *ab initio* and empirical methods, but often the phenomena of interest involve such long length scales that the empirical method is the only practical choice. Of course, effects which are quantum mechanical by nature cannot be described by a classical approach, e.g., buckling of dimers on Si(001) will not be present in empirical results. Nevertheless, when combined with advanced Monte Carlo techniques,[4] empirical potentials are extremely useful for studies of various temperature-dependent large-scale properties.

In this work, we compare the suitability of the Stillinger-Weber[5] (SW), Tersoff-2[6] ($T2$), and Tersoff-3[7,8] ($T3$) potentials for finite-temperature simulations of the Si(001) surface. Few comparative studies of empirical silicon potentials have appeared in the literature, and, in general, only static properties (i.e., $T=0$ K) have been considered in them. Six empirical potentials were tested by Balamane *et al.*, who predicted that SW, $T3$, and to a lesser extent $T2$ would all be useful in simulations involving Si(001).[9] We show that reasonable performance at $T=0$ K does not ensure that a given potential is suitable for finite-temperature simulations. The potentials are thoroughly tested in their ability to describe the basic 2×1 reconstruction and defect structures such as antiphase boundaries and dimer vacancies. Our study reveals unexpected shortcomings and emphasizes the importance of testing potentials for different kinds of applications.

This paper is organized as follows. The potentials are described in the following section. In Sec. III, we give details of the computational procedure. The results and discussion are presented in Sec. IV. Finally, we give our concluding remarks in Sec. V.

II. POTENTIALS

A. The Stillinger-Weber potential (SW)

The Stillinger-Weber potential models bonding with classical two- and three-body interactions. The structural energy of the system is given by the potential-energy function written as

$$E=\sum_{\langle i,j\rangle}\epsilon F_2\left(\frac{r_{ij}}{\sigma}\right)+\sum_{\langle i,j,k\rangle}\epsilon\lambda F_3\left(\frac{r_{ij}}{\sigma},\frac{r_{ik}}{\sigma}\right)\left(\cos\theta_{ijk}+\frac{1}{3}\right)^2, \tag{1}$$

where the first sum is taken over all nearest-neighbor bonds $\langle i,j\rangle$ and the second sum over all triplets $\langle i,j,k\rangle$ with the vertex at site i (j and k are nearest neighbors of i). ϵ and σ are the energy and length units. θ_{ijk} is the angle between $\mathbf{r}_{ij}$ and $\mathbf{r}_{ik}$. The spatial dependence of the two-body interaction in Eq. (1) is introduced through the function F_2 as follows:

$$F_2(y)=\begin{cases}A\left(\dfrac{B}{y^p}-\dfrac{1}{y^q}\right)e^{\delta/(y-b)} & \text{if } y<b\\ 0 & \text{otherwise.}\end{cases} \tag{2}$$

Note that $F_2(y)$ is a function of the rescaled bond length y only, and it vanishes without discontinuities at $y=b$. This function exhibits a minimum equal to -1 at $y=2^{1/6}$, i.e., the ideal bond length is given by $R_0=2^{1/6}\sigma$. The three-body function F_3 is given by

$$F_3(y_1,y_2)=\begin{cases} e^{\gamma/(y_1-b)+\gamma/(y_2-b)} & \text{if } y_1,y_2<b \\ 0 & \text{otherwise,} \end{cases} \tag{3}$$

where y_1 and y_2 are the rescaled lengths of bonds between a central atom i and its two nearest-neighbors j and k.

Originally the parameters of the SW model were fitted to the lattice constant and cohesive energy of the diamond structure with the additional requirement that the melting point and the structure of liquid silicon be described. The original parameters give the value -4.34 eV for the bulk cohesive energy of diamond silicon. As in Ref. 9, we find it convenient to have a common basis for comparison purposes. Therefore, the two- and three-body energy parameters are multiplied by the same scale factor of 1.068 to reproduce the current experimental value -4.63 eV for the cohesive energy. The parameters for the SW model used in this study are[5,9]

$$A=7.0496,\quad B=0.602\,22,\quad p=4,\quad q=0,$$

$$\delta=1,\quad b=1.80,\quad \lambda=21.0,\quad \gamma=1.20,$$

$$R_0=2.351\ \text{Å},\quad \epsilon=2.315\ \text{eV}. \tag{4}$$

B. The Tersoff potentials (T2 and T3)

The Tersoff potentials[6] $T2$ and $T3$ (Refs. 7 and 8) refer to two different parametrizations of the same functional form. Potentials of the Tersoff type are called cluster functionals.[9] Bonding is modeled with pairwise interactions where the attractive term depends on the local environment of the atoms effectively including many-body interactions. The structural energy has the form[8]

$$E=\frac{1}{2}\sum_{i,j}{}' f_c(r_{ij})[Ae^{-\lambda_1 r_{ij}}+b_{ij}Be^{-\lambda_2 r_{ij}}], \tag{5}$$

where the prime indicates that the summation is taken over distinct indices.

The cutoff function of Eq. (5) is given by

$$f_c(r)=\begin{cases} 1 & \text{if } r<R \\ \frac{1}{2}+\frac{1}{2}\cos[\pi(r-R)/(S-R)] & \text{if } R<r<S \\ 0 & \text{if } R>S, \end{cases} \tag{6}$$

and

$$b_{ij}=(1+\beta^n\xi_{ij}^n)^{-1/2n}, \tag{7}$$

$$\xi_{ij}=\sum_{k\neq i,j} f_c(r_{ik})g(\theta_{ijk})\exp[\lambda_3^3(r_{ij}-r_{ik})^3], \tag{8}$$

TABLE I. Parameters for the Tersoff potentials $T2$ and $T3$ for silicon. From Ref. 7.

	$T2$	$T3$
A (eV)	3.2647×10^3	1.8308×10^3
B (eV)	9.5373×10^1	4.7118×10^2
λ_1 (Å^{-1})	3.2394	2.4799
λ_2 (Å^{-1})	1.3258	1.7322
β	3.3675×10^{-1}	1.0999×10^{-6}
n	2.2956×10^1	7.8734×10^{-1}
c	4.8381	1.0039×10^5
d	2.0417	1.6218×10^1
h	0.0000	-5.9826×10^{-1}
λ_3 (Å^{-1})	1.3258	1.7322
R (Å)	2.8	2.7
S (Å)	3.2	3.0

$$g(\theta)=1+c^2/d^2-c^2/[d^2+(h-\cos\theta)^2], \tag{9}$$

where θ_{ijk} is the angle between $\mathbf{r}_{ij}$ and $\mathbf{r}_{ik}$, and the function b_{ij} is the feature which includes the many-body effect, thus, representing a measure of bond order. In addition, terms which limit the range of interaction are also included in b_{ij}.

The parameters for $T2$ were fitted to a database consisting of cohesive energies of real and hypothetical structures of bulk silicon, along with the bulk modulus and bond length of the diamond structure. In the case of $T3$, the parameters were also required to produce the three elastic constants of silicon within 20%. The parameter values for both $T2$ and $T3$ are summarized in Table I.

III. SIMULATION METHOD

Large-scale constant-pressure Monte Carlo (MC) simulations[4] are used in this work to study the properties of the Si(001) surface at finite temperatures. In addition, the structural energies of antiphase configurations are determined using static calculations in which the total energy of the system is minimized using the conjugate gradient method. The MC approach was chosen because, for our purposes, it offers several advantages over other alternative methods such as molecular dynamics (MD). The standard MC method can be substantially accelerated by implementing advanced MC moves into the regular algorithm. For example, in a newly developed hybrid MC-MD scheme, we have implemented multiparticle moves which allow us to study phenomena such as formation or relaxation of two-dimensional islands on Si(001).[10] Since the outcome of the simulations depends crucially on the choice of potential, a comparative study was necessary.

In the MC simulations, the Si(001) system is initially set up as a slab containing 19 or 20 layers of atoms with a surface size of 16×16 or 20×20 atoms. In order to examine finite-size effects, larger slab thicknesses up to 100 atomic layers and surface sizes up to 64×64 atoms are used in some cases. The simulation unit cell is constructed along the [110],

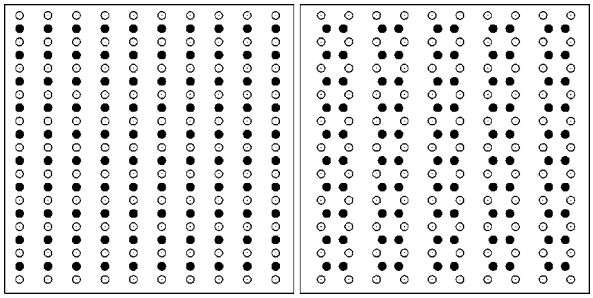

FIG. 1. 2×1 reconstruction of Si(001). The surface is viewed from above. Filled circles mark atoms in the surface layer and the open circles in the layer below. Initial configuration with all atoms in diamond lattice positions is shown on the left. The figure on the right shows a fully dimerized surface obtained from an MC simulation with multiparticle moves using the SW potential (Ref. 10).

$[1\bar{1}0]$, and [001] directions. Periodic boundary conditions are applied in the *x* and *y* directions. The structural energy of the system, *E*, is calculated from the atomic coordinates using the SW, *T*2, or *T*3 potential.

At each MC step, we choose a particle at position $\mathbf{r}_i$ and attempt to displace it by a small amount to position $\mathbf{r}_i'$. The acceptance probability of the move is given by the Metropolis form[11] using the structural energy *E* to calculate the energy difference associated with the displacement of atom *i*. The pressure is kept constant at $P=0$ by allowing the sides of the simulation cell to fluctuate independently. Every $N_{\rm vol}$ MC steps (typically $N_{\rm vol}=10$), we randomly choose new linear sizes for the system (L_x',L_y',L_z'), slightly altered from the previous ones. The positions of the atoms are scaled by the relative change in the linear system size: $x'=xL_x'/L_x$, $y'=yL_y'/L_y$, and $z'=zL_z'/L_z$. The acceptance probability for the volume change is calculated from the Metropolis form using an effective Hamiltonian given by[12]

$$H_{\rm eff}=E-Nk_{\rm B}T\ln(L_xL_yL_z). \tag{10}$$

Unless otherwise indicated, the results presented in Sec. IV were obtained from sufficiently long simulation runs to obtain error bars smaller than or comparable to the size of the corresponding symbol.

IV. RESULTS

A. 2×1 reconstruction

The experimental value for the silicon lattice constant at room temperature (300 K) is 5.43 Å, which means that the nearest-neighbor separation in bulk is 2.35 Å.[13] When a silicon crystal is cut along the (001) plane, the surface atoms are left with two unsaturated bonds (dangling bonds) each. At the expense of introducing a large surface stress, the Si(001) surface reconstructs to form rows of dimerized atoms, yielding a 2×1 unit cell. (See Fig. 1). The reconstruction reduces the number of dangling bonds per atom from two to one and establishes two characteristic directions on the surface: parallel and perpendicular to the dimer rows. The surface is under tensile stress along the dimer bond, while in the perpendicular direction it is under compressive stress. The dimer bond length has been measured to be close to the bulk bond length and the surface remains dimerized up to temperatures of at least 1475 K.[14]

Static calculations by Balamane and co-workers[9] show that the 2×1 reconstruction lowers the energy of the Si(001) surface with respect to an unreconstructed surface for all three empirical potentials considered in this study. Finding the global minimum, however, is not a straight-forward task,

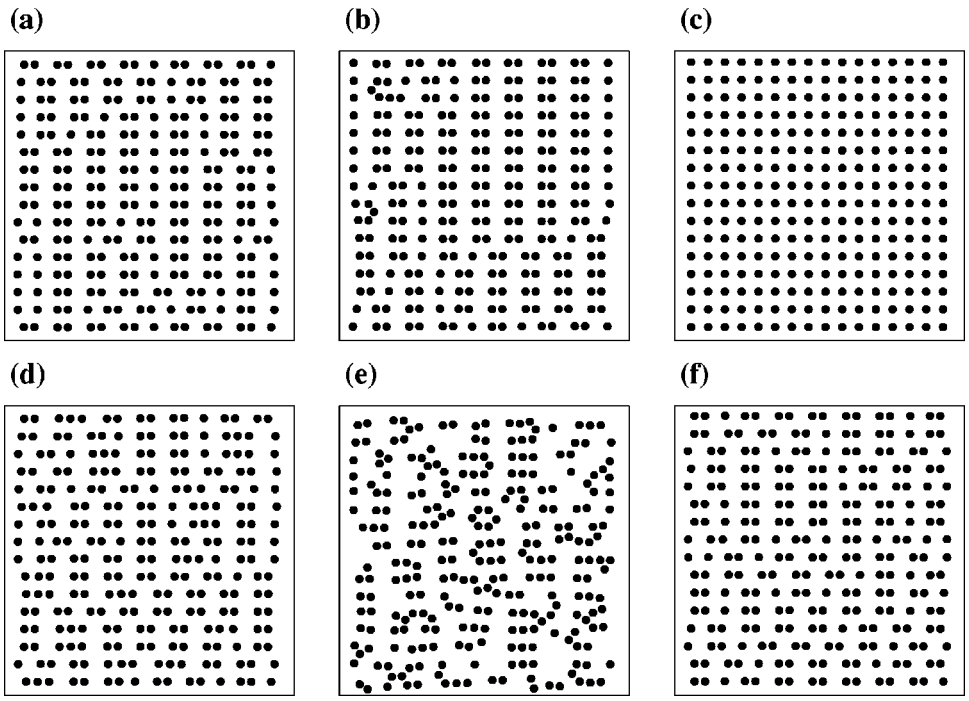

FIG. 2. Typical *metastable* surface configurations obtained from a regular MC run at $T=116$ K (upper row) and at $T=812$ K (lower row) using the SW potential (a) and (d), the *T*2 potential (b) and (e), and the *T*3 potential (c) and (f). The configurations are averages over 20 000 MC steps after initial run of 20 000 MC steps. All atoms were initially placed in diamond lattice positions.

because systems with complicated energy landscapes, like the Si(001) surface, can have multiple metastable states.

Figure 2 shows typical *metastable* configurations that are generated in an MC simulation when the surface atoms are initially in ideal diamond lattice positions (1×1 ordering shown on the left in Fig. 1). The configurations are averages over 20 000 MC steps after 20 000 equilibration steps. For clarity, only the surface atoms are shown. In the upper row configurations the simulation temperature was $k_BT=0.01$ eV (116 K) and the lower row configurations were obtained at $k_BT=0.07$ eV (812 K). Note that these configurations do not correspond to the state of lowest free energy, but on the time scale of a usual simulation, they remain relatively unchanged. The system is trapped in a metastable state because breaking up a dimer requires a large amount of energy and the formation of a perfectly dimerized surface would require many such unlikely events. In the MC approach, equilibration can be accelerated using advanced simulation techniques described in Sec. III. [The fully dimerized Si(001) surface shown on the right in Fig. 1 was generated using an algorithm with multiparticle moves.]

For the purpose of the current study, the metastable configurations of Fig. 2 provide information on the properties of the different empirical potentials. At the lower temperature, the SW [Fig. 2(a)] and $T2$ [Fig. 2(b)] potentials produce similar structures: segments of dimer rows with undimerized atoms in between. On the other hand, when the $T3$ potential is used [Fig. 2(c)], a large energy barrier prevents spontaneous dimerization at low temperatures and consequently the surface atoms remain in their diamond lattice positions. For the SW and $T2$ potentials, the first dimers form at random positions. Once formed, the existing dimers influence the dimerization of surrounding atoms, so that sections of dimer rows form on the surface. This implies that the formation of straight-dimer rows is energetically favorable for these two potentials. When two dimerized sections of the surface meet, there is a 50% chance that the 2×1 reconstruction of one section is in phase with the other section. In this case, the two domains can coalesce without defects. On the other hand, if the positions of the dimer rows in one section are shifted by one lattice constant with respect to the other section, then an antiphase boundary (APB) forms where the two domains join. APB sections are visible in both Figs. 2(a) and 2(b).

At the higher temperature, the surface produced by the SW potential [Fig. 2(d)] is more disorganized than at the lower temperature. In addition to dimers and single atoms, many trimers are also visible on the surface. This indicates that the trimer configuration is energetically more favorable than having a single atom with two dangling bonds. Trimers are not observed at lower temperatures, because the formation of a trimer requires concerted motion of multiple surface and substrate atoms. The resulting energy barrier can only be overcome with sufficient thermal motion. Note that these trimers are metastable and serve as an intermediate state in the computational procedure.

Figure 2(e) reveals a serious limitation of the $T2$ potential: the surface becomes very unorganized and eventually melts at a temperature clearly below the experimentally determined melting point of silicon[15] (1683 K). This problem is most likely caused by the overly soft bond-bending forces of the $T2$ model. Note that the melting happens regardless of the initial configuration of the simulation (e.g., even if a perfect 2×1 reconstruction is initially placed on the surfaces). The $T3$ potential was constructed to improve the elastic properties of the Tersoff model compared to the earlier $T2$ parametrization. Figure 2(f) shows the configuration produced by the $T3$ potential at the higher temperature. The atomic arrangement resembles that of the SW and $T2$ potentials at the lower temperature with the exception that straight-dimer row segments are clearly shorter. This is because the $T3$ potential in fact favors antiphase configurations (see Sec. IV D 1 for details).

B. Effects of finite slab thickness

In simulational studies involving surfaces, the effects of the surface have generally been assumed to extend only a few atomic layers into the bulk. In principle, this is true if we consider a surface on an infinite substrate: deviations from bulk values decrease rapidly as a function of distance from the surface. Following this argumentation, a 20-layer thick slab should be sufficiently thick to prevent the two surfaces from interacting with each other. We found, however, that in a constant-pressure simulation where the sides of the simulation slab are allowed to fluctuate independently, the surfaces cause significant finite-size effects due to the finite thickness of the slab. The effects caused by finite cross-sectional area are much smaller because periodic boundaries are used in the x and y directions. Nevertheless, these can also be significant when making very accurate calculations.

In this section, we discuss how the anisotropic 2×1 reconstruction of the Si(001) surface leads to unphysical behavior in a finite-temperature simulation. We propose a solution that clearly improves the situation but also point out that problems may arise in all simulations in which similar methods are used. Figure 3 shows the average separation between atomic layers in z direction (perpendicular to the surfaces) at (a) $k_BT=0.01$ eV (116 K) and (b) $k_BT=0.05$ eV (580 K). The two surfaces of the slab are identical, both are 2×1 reconstructed with dimer bonds in the x direction. For all three potentials, we observe oscillatory behavior in the layer separations through the whole bulk region of the slab. The amplitude of the oscillations does not decrease with distance from the surface as would be expected of a regular surface effect. The oscillations produced by the SW and $T3$ potentials are not affected by change in temperature (except for a slight increase in all distances due to thermal expansion). In the case of the $T2$ potential, the system undergoes a ''phase shift'' with increasing temperature where large distances become smaller and vice versa. The surface begins to melt at temperatures above 200 K due to the overly soft bond-bending forces of the $T2$ potential. The distortion of the 2×1 reconstruction is reflected through the whole system and causes the changes in the layer separations.

This leads us to the origin of the oscillations. It should be noted first that in bulk simulations (i.e., if periodic boundaries are used in all three directions) we do not observe such

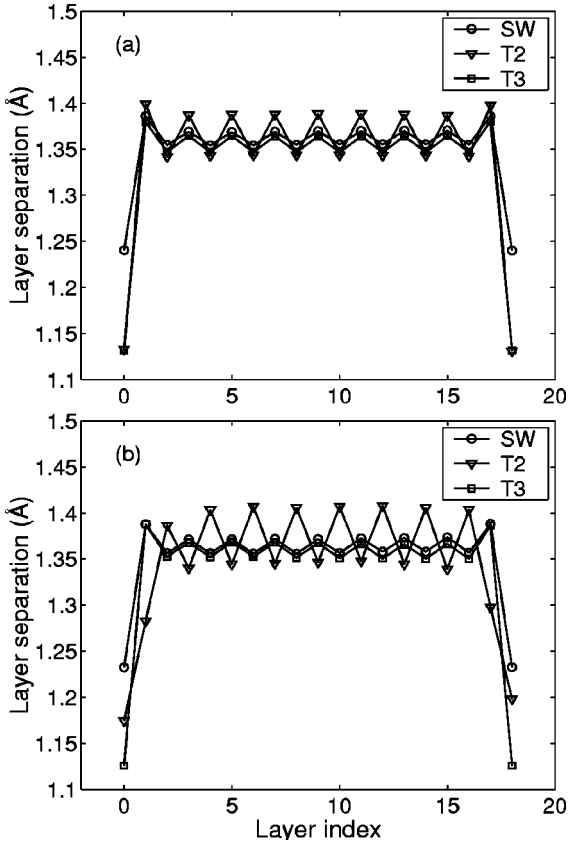

FIG. 3. Separation of atomic layers in z direction for SW, $T2$, and $T3$ at (a) $k_BT=0.01$ eV (116 K) and (b) $k_BT=0.05$ eV (580 K). The x axis marks the number of atomic layers when traversing the slab in z direction. The error bars for the SW and $T2$ data are smaller than the size of the corresponding symbols. For the $T2$ data, the error bars are somewhat larger, $\approx 2-3$ times the size of the symbols.

behavior. In addition, increasing the cross-sectional area of the simulation slab does not affect the amplitude of the oscillations (simulations were carried out using surface sizes up to 64×64 atoms while keeping the slab thickness constant). In Fig. 4, the amplitude of the oscillations (in the bulk section of the slab) is plotted as a function of bulk thickness. We note that the amplitude decreases with increasing bulk thickness, which indicates that the oscillations are caused by the surfaces due to finite slab thickness. We also observe that in the simulations the system shrinks in the x direction (in the direction of the dimer bonds on both surfaces), while it expands in the y direction. It is reminded that the 2×1 reconstructed Si(001) surface is under tensile stress in the direction of the dimer bond and under compression in the perpendicular direction. In a constant-pressure MC simulation at $P=0$, the sides of the simulation slab fluctuate independently. The system attempts to relieve part of the stress by the anisotropic change in L_x and L_y, which causes the atomic layers in the diamond lattice to move in such a way that every other interlayer distance becomes smaller and every other larger. The energy gain from relieving the stress of the surface is balanced by the energy cost from distorting the

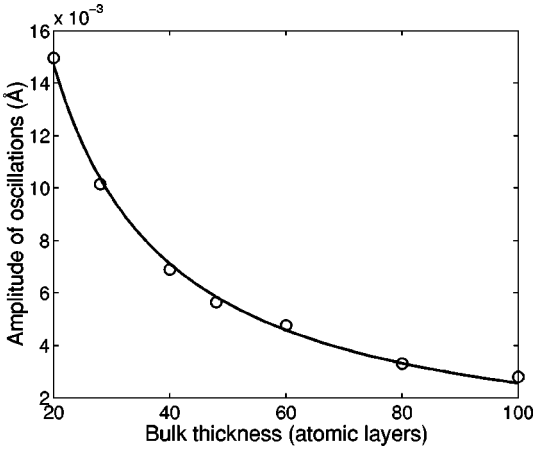

FIG. 4. Amplitude of oscillations in layer separation for the SW model as a function of bulk thickness. The solid curve is an inverse function fitted to the data. The simulation temperature is $k_BT=0.03$ eV (348 K). Due to increasingly long simulation times, the error bars for bulk thicknesses larger than 20 layers are of the order 2×10^{-3}.

diamond lattice in the bulk. The influence of the surfaces is inversely proportional to the bulk thickness.

In order to confirm our theory, we performed static calculations in which either an isotropic or anisotropic strain was applied in the x and y directions. The results show that the layer separations in bulk silicon are constant if the system is under isotropic strain, whereas anisotropic strain produces similar oscillations as are observed in the MC simulations. The larger the anisotropy, the larger the amplitude of the oscillations is.

The finite slab thickness affects the simulation results in a significant way: for example, the dimer bond length increases as a function of bulk thickness. We cannot solve this problem by increasing the slab thickness, because even hundred atomic layers do not give convergence to acceptable accuracy. We can, however, rotate the orientation of the dimer bonds on one of the surfaces by using an odd number of atomic layers in the simulation slab. Due to the geometry

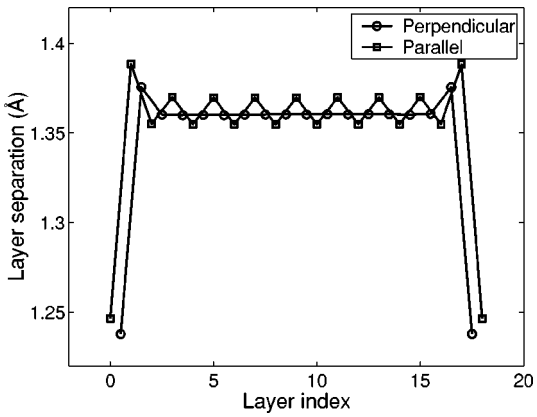

FIG. 5. Layer separations for two systems with one having same dimer orientation on the two surfaces (parallel) and the other perpendicular dimer bonds on the two surfaces. The x axis marks the number of atomic layers when traversing the slab in z direction.

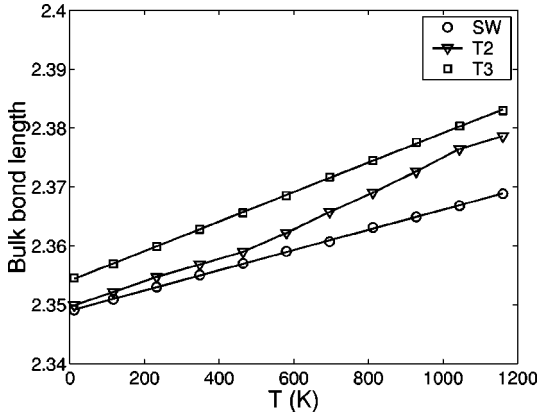

FIG. 6. Bulk bond length as a function of temperature. The symbols are simulation results using the SW (circles), $T2$ (triangles), or the $T3$ (squares) potential. For the SW and $T3$ models, the solid lines are linear fits to the data.

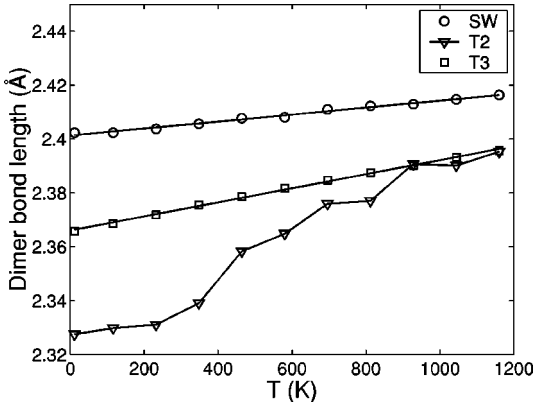

FIG. 7. Dimer bond length as a function of temperature. The symbols are simulation results using the SW (circles), $T2$ (triangles), or the $T3$ (squares) potential. For the SW and $T3$ models, the solid lines are linear fits to the data.

of the diamond lattice, an odd number of atomic layers results in a 2×1 reconstruction on one surface and 1×2 reconstruction on the other.

Figure 5 shows a comparison of layer separations for two systems with one having parallel (20 atomic layers) and the other perpendicular dimer bonds (19 atomic layers) on the two surfaces. We note that if the two surfaces have perpendicular orientations, then the two surface effects cancel out and the interlayer distance no longer oscillates. The same result cannot be achieved by fixing the bottom layers of the slab (using a single surface instead of two surfaces) because the amplitude decreases but the oscillations do not disappear. As a conclusion, the finite-size effects can be considerably reduced by using an odd number of atomic layers (perpendicular surface orientations). We note, however, that the problem cannot be fully solved this way and even subtle effects can influence accurate calculations in a significant way (for further discussion see Sec. IV D).

C. Structural properties

We now focus on the structural properties of the 2×1 reconstruction. Figures 6 and 7 show the bulk and the dimer bond lengths as a function of temperature for the three potentials SW, $T2$, and $T3$. The data are obtained from simulations using a system of $16\times16\times19=4864$ atoms (perpendicular dimer bonds on the lower and the upper surface of the slab). The statistical errors are smaller or of the same size as the symbols used in the figures (the fluctuations in dimer bond lengths are slightly larger due to the small number of dimers). The experimental value of the nearest-neighbor bond length in bulk is ≈2.35 Å at low temperatures and the distance between dimers is estimated to be close to this value.[1] Our simulation results show that all three potentials give bulk bond lengths very close to the experimental value at low temperatures. We note that the thermal-expansion coefficient of the $T2$ data changes around $T=500$ K. This unphysical behavior is explained by the melting of the two surfaces which extends several layers into the bulk. The bulk properties of the system are affected by the melting because of the finite thickness of the simulation slab.

Another point to note is that experiments find a negative thermal expansion at low temperatures ($T<120$ K) which is not correctly modeled by any of the three potentials. For a more detailed discussion see Ref. 12. On the other hand, the dimer bond lengths obtained at low temperatures agree well with the static calculations of Balamane *et al.*,[9] but *ab initio* calculations reviewed in Ref. 9 predict the dimer bond length to be shorter than the bulk bond length. Out of the three potentials considered in this study, only $T2$ shows this strengthening of the dimer bond at low temperatures. The $T2$ model, however, is clearly unsatisfactory at temperatures above 200 K where the dimer bond length increases rapidly as the surfaces begin to melt. The irregular shape of the dimer bond length curve is due to disordering of the surface (see Fig. 2 for details). Because of these shortcomings, the $T2$ potential is not suited for studies of the Si(001) surface at temperatures above 200 K.

D. Surface defects

1. Antiphase boundaries

Experimentally, APB's are only observed under conditions when growth proceeds via island nucleation on stepped surfaces.[1] The growing islands have a 50% chance to nucleate in such a way that an APB forms upon coalescence with the upper terrace. APB's serve as preferential nucleation sites for atoms landing on the upper terrace, which leads to increasing surface roughness. On smooth surfaces (layer-by-layer growth mode) APB's are not observed. Computationally, the formation of dimers on an initially bulk-terminated surface is affected by the local neighborhood of the individual atoms. Using a single ''seed'' row of dimers on an, otherwise, bulk-terminated surface induces straight-row dimerization for the SW and $T2$ potentials at low temperatures (where random dimer formation is slow). For the $T3$ potential, straight dimer rows do not form even when a seed dimer row is used, which indicates that the 2×1 reconstruction is not the ground state predicted by this potential.

The energy difference between an antiphase configuration and an ideal 2×1 reconstruction is extremely small. A static,

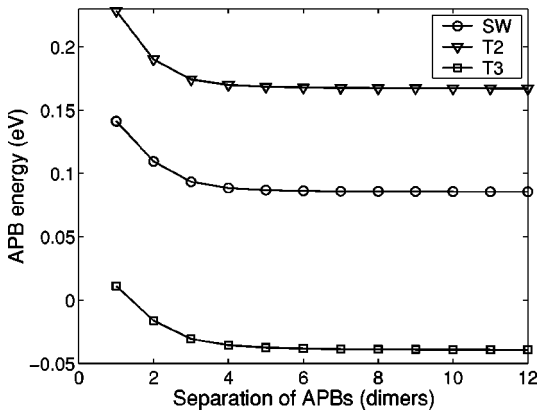

FIG. 8. Excess surface energy per APB as a function of separation of APB's for a unit cell containing two equally sized antiphase domains. The reference point is a 2×1 reconstructed surface.

energy-minimization method was used to calculate the excess surface energy of antiphase configurations with respect to a defect-free 2×1 reconstruction. The unit cell of the calculations was $2n$ dimers long and one dimer wide with two APB's separated by n dimers in the cell ($n=1-100$). The bulk section was 25 atomic layers thick with the bottom layers fixed to diamond lattice positions. Figure 8 shows the excess surface energy per APB as a function of APB separation (expressed in number of dimers, n) for a one dimer wide unit cell. As a check, some APB energies were also calculated using MC simulations at very low temperatures and the results were found to fully agree with the static calculations.

For all three potentials, the energy increases as the APB separation becomes smaller, indicating that the interaction between two APB's is repulsive. The APB energies of all three potentials also converge to meV accuracy at a separation of eight dimers. For the $T3$ potential, the excess surface energy becomes *negative* when the APB's are separated by at least two dimers, which in turn indicates that the straight-row 2×1 reconstruction is a metastable state. This significantly limits the suitability of the $T3$ potential for finite temperature MC simulations where the atoms are not restricted to maintain a preassigned surface configuration.

Table II summarizes the results obtained for the APB configurations. The saturation value and the energy of a zigzag configuration (APB's separated by a single dimer) are compared with tight-binding (TB) results from Ref. 16. The $T2$ potential gives values closest to the TB calculations, but qualitatively both the SW and the $T2$ potential produce a similar energy curve to the one obtained using the TB method (see Ref. 16 for details). The negative values for the $T3$ potential are in clear disagreement with both the TB results and experimental observations of the Si(001) surface.

TABLE II. Energies of an isolated APB ($n>20$) and a zigzag structure ($n=1$) for the SW, $T2$, and $T3$ potentials compared with tight-binding (TB) results (from Ref. 16). The TB saturation value is for $n=8$.

Potential	APB	zigzag
SW	0.0856	0.1414
$T2$	0.1670	0.2285
$T3$	−0.0345	0.0112
TB	0.162	0.190

2. Dimer vacancies

Scanning tunneling microscopy experiments have produced consistent evidence that a high defect density is intrinsic to the (001) surface of silicon.[17] From the theoretical perspective, *ab initio* total-energy calculations by Wang, Arias, and Joannopoulos[18] have shown that dimer vacancies (DV's) and DV complexes are energetically favorable and stable intrinsic defects of the Si(001) surface. It was seen that the rebonding of the exposed second-layer atoms reduces the number of dangling bonds at the expense of introducing a large surface stress. The *ab initio* calculations of Ref. 18 show that the formation energy of a single DV is only 0.22 eV for a rebonded configuration. For DV complexes, the formation energy per DV can be even lower than 0.2 eV.

Exposure to Ni contamination substantially increases the density of dimer vacancies on Si(001).[22] Consequently, the intrinsic interaction between the vacancies leads to the formation of an ordered defect structure with $2\times n$ periodicity. We would like to point out that similar structures are also observed on Si(001) surfaces covered with thin epitaxial layers of Ge.[19] In this case, ordered $2\times n$ patterns are formed in order to relieve part of the lattice-mismatch induced strain system. Total-energy calculations[20,21] show that vacancies have negative formation energies on Ge-covered Si(001) surfaces with respect to a uniformly strained Ge layer. Mixed semiconductor systems are beyond the scope of the current study, but since dimer vacancies obviously play a significant role in various systems involving the Si(001) surface, it is essential to test how well the empirical potentials are able to model such defect structures.

In contrast to the static APB calculations, constant-pressure MC simulations allow us to study whether effects such as the rebonding of second-layer atoms can be spontaneously reproduced by the empirical potentials. In order to compare with static *ab initio* results, the systems were quenched down to a very low temperature (11 K) after a simulation run at a higher temperature (580 K for SW and $T3$, 116 K for $T2$). Averages were calculated after equilibration at the lower temperature. As a check, static results for the 2×1 reconstruction from Ref. 9 are included in Table III. We note that the surface energies show a slight systematic increase due to finite temperature used in the MC simulations, but the difference between static and low-temperature results is very small.

Figure 9 shows the difference in average energy per particle with respect to a defect-free 2×1 reconstruction for a vacancy structure with 2×10 periodicity. The energies are given as a function of distance from the surface (in atomic layers) at $T=11$ K. We note that for the SW and $T3$ potentials, the average energy of the dimers increases by a small amount, whereas the $T2$ potential predicts that the energy change is clearly *negative* for the surface layer. For SW and $T2$, the energy of the second-layer atoms increases by less than 0.1 eV due to rebonding. $T3$ gives a larger increase in

TABLE III. Surface energies (γ) and formation energies (E_f) of dimer vacancy configurations. The surface energies are given in eV per 1×1 cell. The formation energies are calculated with respect to the 2×1 surface and are given in eV per DV. ΔE_f is the difference in formation energies between a nonrebonded (metastable) and rebonded (stable) configuration (for the 2×5 reconstruction). The static results for the empirical potentials are from Ref. 9. The DFT results for the $2\times n$ reconstruction are from Ref. 23 ($n=1$), Ref. 24 ($n=4$), and Ref. 18 ($n=5$). The surface energies of the $2\times n$ structures were calculated from relative energies by comparing to the surface energy of the 2×1 reconstruction from Ref. 23.

	DFT	SW	*T*2	*T*3
$\gamma(2\times1)$	1.57	1.412	0.752	1.363
static		1.416	0.757	1.367
$\gamma(2\times10)$		1.418	0.714	1.431
$\gamma(2\times5)$	1.59	1.451		
$\gamma(2\times4)$	1.61	1.492		
$E_f(2\times10)$		0.13	−0.76	1.35
$E_f(2\times5)$	0.22	0.40		
$E_f(2\times4)$	0.28	0.64		
ΔE_f	0.42	1.45		

energy because the second-layer atoms do not rebond spontaneously even at 580 K. This nonrebonded configuration is a metastable state which for the *T*3 potential lies in a deep potential well. This can be seen by comparing with the static results in Ref. 9. For a rebonded 2×4 structure, they obtain the value 0.62 eV for the formation energy per DV, which is clearly below our value 1.35 eV for the nonrebonded structure (see Table III).

The surface energy per unit area γ is defined as

$$\gamma=\frac{1}{A}(E_{\mathrm{tot}}-NE_c), \tag{11}$$

where E_{tot} is the total energy of the system composed of N atoms with bulk cohesive energy E_c per atom (determined from a simulation with 2×1 reconstructed surfaces) and A is the area of the exposed surface (note that there are two surfaces in the simulation slab). To calculate the formation energy E_f the surface energy of each system containing the DV structure is compared to the surface energy of a defect-free 2×1 reconstruction. This is equivalent to comparing the total energies with the bulk total energy as the chemical potential (or having the source and sink of atoms at the edge of a step on the surface).

Table III summarizes the results obtained for the DV structures. There is uncertainty in the last digits of the given values because the calculations involve very small (meV) energy differences. Determining very small differences accurately can be difficult because of similar effects due to finite slab thickness as discussed in Sec. IV B. In order to estimate the errors, we performed test runs using larger bulk thicknesses up to 59 layers and larger cross-sectional areas up to 30×30 atoms. The surface energy values increase slightly when thicker slabs are used and larger cross-sectional areas

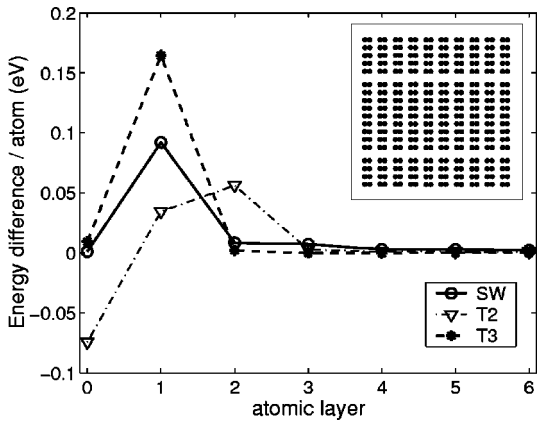

FIG. 9. Average energy difference per atom with respect to an ideal 2×1 reconstruction for a 2×10 reconstructed surface. The x axis denotes distance from the surface. The inset shows the atomic arrangement of the surface atoms in the 2×10 configuration.

lead to somewhat smaller values. These systematic deviations are the result of small changes in the structure of the simulation cell which are determined by the relative thickness of the simulation slab with respect to the cross-sectional area. For the surface energies given in Table III, the errors are estimated to be less than 10 meV. These deviations do not, however, affect the relative order of the surface energies obtained for the different vacancy structures. Thus, the qualitative conclusions that are drawn from the results remain unchanged even if the absolute values are not fully accurate. Nevertheless, the questions related to the finite-size effects in finite-temperature simulations need careful attention and we plan to investigate them more thoroughly in our future work.

For the defect-free 2×1 reconstruction, the SW and *T*3 potentials give surface energies in fair agreement with the discrete Fourier transform (DFT) value, whereas the value for *T*2 is clearly too small. The *T*2 potential also predicts that vacancy formation is exothermic with respect to the 2×1 reconstruction; the formation energy per DV for the 2×10 vacancy-line structure is -0.76 eV. As already mentioned, the *T*3 potential produces such a large energy barrier for rebonding of the second-layer atoms that the system remains in a nonrebonded metastable state at $T=580$ K. This leads to the large formation energy of 1.35 eV.

The SW potential was examined in more detail due to its satisfactory overall performance. The central features of dimer vacancies, rebonding of second-layer atoms and atomic displacements in the vicinity of the defect, are also described with reasonable accuracy by SW. The formation energies of dimer vacancies in periodic $2\times n$ structures agree fairly well with corresponding *ab initio* results. To compare the energy difference between a metastable, nonrebonded configuration and the stable rebonded configuration, a simulation using the SW potential was performed at a very low temperature (11 K) where the second-layer atoms are unable to rebond due to lack of thermal motion. The SW potential gives the value 1.45 eV, which is clearly higher than the corresponding DFT value 0.42 eV obtained in Ref. 18. The discrepancy between the SW and DFT values is most likely

caused by the fact that empirical potentials, in general, do not give accurate descriptions of surface stress;[9] although the atomic displacements are qualitatively similar to those calculated by *ab initio* methods, it is not surprising that quantitative results do not fully agree. Furthermore, it is difficult to estimate the accuracy of the *ab initio* results because varying techniques and input parameters have been used by different groups. Structural parameters can usually be determined with good accuracy but energies converge more slowly below plane-wave cutoff energy[9] of 10 Ry. Typically, values less than 10 Ry have been used for computational reasons. It is important to keep this in mind when making comparisons.

One interesting point that should be noticed from the results of Table III is the dependence of the formation energy on the periodicity of vacancy-line structure. The smaller the value of n, the larger is the formation energy per DV for the $2\times n$ configuration. This indicates that the dimer vacancy lines interact repulsively in the direction perpendicular to the dimer bonds. In the other direction, along the dimer bonds, the interaction must be short ranged and attractive due to the fact that the DV are observed to organize into rows.

V. CONCLUSION

We have performed a comparative study of empirical potentials of silicon with emphasis on finite-temperature simulations of the Si(001) surface. The results show that a reasonably accurate description of bulk properties does not ensure that a potential is suitable for simulations involving surfaces. In addition, simulations at finite temperatures can be problematic even if the potential gives good results at $T=0$ K.

The SW potential was found to give the best overall performance in describing the main properties of the Si(001) surface: dimer formation, stability of the straight-row 2×1 reconstruction, bond lengths, etc. Surface defects such as dimer vacancies and periodic vacancy-line structures are also described fairly accurately. The results are not in qualitative disagreement with any current experimental or theoretical findings of the Si(001) surface, although all details are not correctly modeled.

In contrast, the $T2$ and $T3$ potentials both suffer from serious limitations in their description of the Si(001) surface. The $T2$ potential gives fairly good results at low temperatures ($T<200$ K) but at higher temperatures the potential displays clearly unphysical behavior as the surface melts after 500 K. The $T2$ potential also predicts that vacancy formation is exothermic with respect to a defect-free 2×1 reconstruction which is in disagreement with *ab initio* results. The $T3$ potential was found to favor antiphase domains over the experimentally observed 2×1 reconstruction. These results limit the suitability of the Tersoff potentials for finite-temperature simulations where the surface atoms are not confined to the immediate vicinity of their initial positions.

In addition to studying the properties of the empirical potentials, we found that significant finite-size effects can be encountered in constant-pressure simulations involving surfaces. These observations are not limited to simulations of silicon surfaces but apply to all those cases where similar simulation methods are used. We propose a solution to relieve part of the problem but emphasize the importance of paying attention to these questions.

In conclusion, we have found significant differences in the performance of three widely used empirical silicon potentials: SW, $T2$, and $T3$. None of them can give a fully accurate description of the Si(001) surface, but in our opinion, the SW potential is best suited for simulations conducted at finite temperatures. We believe that despite its shortcomings, the SW potential can be used in large-scale simulations of the Si(001) surface to study otherwise intractable problems. For example, we are currently developing MC techniques to study the structure of thin Ge layers on Si(001). Although time consuming, it is always worthwhile to test the suitability of a potential for a given application because empirical potentials are never fully transferable. Hopefully, this investigation will prove useful for other researchers planning to use these potentials in their work.

ACKNOWLEDGMENTS

This work was supported in part by the Academy of Finland, project on Computational Research of Semiconductor Materials, Project No. 1169043 (Finnish Center of Excellence Program 2000-2005), and in part by NSF, Grant No. DMR-0094422. L.N. would also like to acknowledge support of the Finnish Cultural Foundation.

[1] B. Voigtländer, Surf. Sci. Rep. **43**, 127–254 (2001).
[2] M.C. Payne, M.P. Teter, D.C. Allan, T.A. Arias, and J.D. Joannopoulos, Rev. Mod. Phys. **64**, 1045 (1992).
[3] C.M. Goringe, D.R. Bowler, and E.H. Hernández, Rep. Prog. Phys. **60**, 1447 (1997).
[4] D. P. Landau and K. Binder, *A Guide to Monte Carlo Simulations in Statistical Physics* (Cambridge University Press, Cambridge, 2000).
[5] F.H. Stillinger and T.A. Weber, Phys. Rev. B **31**, 5262 (1985).
[6] J. Tersoff, Phys. Rev. B **37**, 6991 (1988).
[7] J. Tersoff, Phys. Rev. B **38**, 9902 (1988).
[8] J. Tersoff, Phys. Rev. B **39**, 5566 (1989).
[9] H. Balamane, T. Halicioglu, and W.A. Tiller, Phys. Rev. B **46**, 2250 (1992).
[10] F. Tavazza, L. Nurminen, D. P. Landau, A. Kuronen, and K. Kaski (to be published).
[11] N. Metropolis, A.W. Rosenbluth, M.N. Rosenbluth, A.H. Teller, and E. Teller, J. Chem. Phys. **21**, 1087 (1953).
[12] M. Laradji, D.P. Landau, and B. Dünweg, Phys. Rev. B **51**, 4894 (1995).
[13] J. Singh, *Physics of semiconductors and their heterostructures* (McGraw-Hill, New York, 1993).
[14] H.J.W. Zandvliet, Rev. Mod. Phys. **72**, 593 (2000).
[15] J.Q. Broughton and X.P. Li, Phys. Rev. B **35**, 9120 (1987).

[16] D.R. Bowler and C.M. Goringe, Phys. Rev. B **58**, 3937 (1998).
[17] R.M. Tromp, R.J. Hamers, and J.E. Demuth, Phys. Rev. Lett. **55**, 1303 (1985).
[18] J. Wang, T.A. Arias, and J.D. Joannopoulos, Phys. Rev. B **47**, 10 497 (1993).
[19] F. Liu, F. Wu, and M.G. Lagally, Chem. Rev. **97**, 1045 (1997).
[20] J. Tersoff, Phys. Rev. B **45**, 8833 (1992).
[21] F. Liu and M.G. Lagally, Phys. Rev. Lett. **76**, 3156 (1996).
[22] J.-Y. Koo, J.-Y. Yi, C. Hwang, D.-H. Kim, S. Lee, and D-H. Shin, Phys. Rev. B **52**, 17 269 (1995).
[23] I.P. Batra, Phys. Rev. B **41**, 5048 (1990).
[24] N. Roberts and R.J. Needs, Surf. Sci. **236**, 112 (1990).